A pilot magnetotelluric survey for geothermal exploration in Mae Chan region, northern Thailand

Puwis Amatyakul, Tawat Rung-Arunwan, Weerachai Siripunvaraporn*

Department of Physics, Faculty of Science, Mahidol University, 272 Rama 6 Road, Rachatawee, Bangkok 10400, Thailand

ARTICLE INFO

ABSTRACT

There are many potential sites for geothermal power plants in Thailand. After many years of geological and geophysical surveys, a pilot magnetotelluric (MT) survey was made to assess the reservoir of the Mae Chan geothermal area, northern Thailand, which is one of the key areas for geothermal development. Seven MT sites were deployed in a 3 km × 4 km area around the Mae Chan district covering the Mae Chan hot springs. The MT data were acquired at low and high frequency ranges and were inverted using a 3-D MT inversion to yield the 3-D resistivity structure of the area. The results show that there are two conductive zones near the surface associated with the hot fluid of the Mae Chan hydrothermal system. The hot fluid reservoir mostly resides at less than 500 m below the surface in weathered and fractured granite and in the overlying sedimentary deposits. Its source rock is imaged as a resistive zone corresponding to the hot granite batholith below it. The hot fluid rises up along the Mae Chan fault. The fault is clearly observed as a resistivity contrast extending from the surface to depth. It dips at a moderate angle. From the measured temperature of the fluid from a drill hole and the estimated temperature of the granite rock from the resistivity structure we conclude that the Mae Chan geothermal area is likely to be suitable for immediate development of a small-scale geothermal power plant.

1. Introduction

To reduce Thailand's growing dependence on fossil fuels, finding alternative sources of energy is vital for the Thai economy. Geothermal energy has become a choice for many countries around the world during the past few decades because of its low cost and low emissions. Northern Thailand is one of the areas where the potential for geothermal power plants is very high (Barr et al., 1979; Chuaviroj, 1988; Owens, 2012; Singharajwarapan et al., 2012). Many of the hot springs in northern Thailand (Fig. 1a) have a temperature exceeding 80 °C (Chuaviroj, 1988; Singharajwarapan et al., 2012; Subtavewung et al., 2005). These hot springs are commonly associated with strike-slip fault zones (Fig. 1a) such as the Mae Chan Fault (MCF), the Mae Hong Son Fault (MHF), and the Pha Yoa Fault. These faults formed as the Indian plate subducted beneath the Eurasian plate. Currently, only one geothermal power plant is operating in Thailand. It is a 0.3 MW Ormat binary power plant installed in 1989 in the Fang district of Chiang Mai province in northern Thailand (Fig. 1). The plant utilizes 130 °C

water encountered in fractured granite at depths of 250–400 m (Ramingwong et al., 2000).

Another prominent area classified by the Thailand Department of Alternative Energy Development and Efficiency (DEDE) is the Mae Chan geothermal field (Raksaskulwong, 2008; Ramingwong et al., 2000), located about 30 km to the north of Chiang Rai province (Fig. 1b). The Mae Chan area along with the survey sites is shown in Fig. 2. The hot springs at Mae Chan are associated with the almost east-west left-lateral strike-slip Mae Chan Fault (Figs. 1b and 2), which extends from the northernmost part of Thailand near the Thailand–Myanmar border through the Mae Chan region to the Mekong River into Laos, a distance of 140 km. The thermal waters at Mae Chan seep into the base of the Mae Chan creek, which is only exposed during the dry season (shown as Y1 and Y4 in Fig. 2). They also form hot pools at Y3a and Y3b (Fig. 2) in which the measured temperatures can reach 99.5 °C (Singharajwarapan et al., 2012). In addition, hot springs have been reported near MCH3 (Fig. 2).

The Mae Chan region is located at the boundary between a valley filled with Quaternary alluvium to the east and a Triassic granitic batholith to the west (Fig. 1b). Permian–Triassic rhyolite and ash-flow tuff can be found in the northeastern part of the Mae Chan area, and low-grade metamorphic rocks consisting of phyllite, quartzite, and schist formed during Devonian–Carboniferous time occur in the northwestern part of the area (Fig. 1b). It has been suggested

* Corresponding author. Tel.: +66 2 2015764; fax: +66 2 3547159.
  E-mail address: wsiripun@gmail.com (W. Siripunvaraporn).
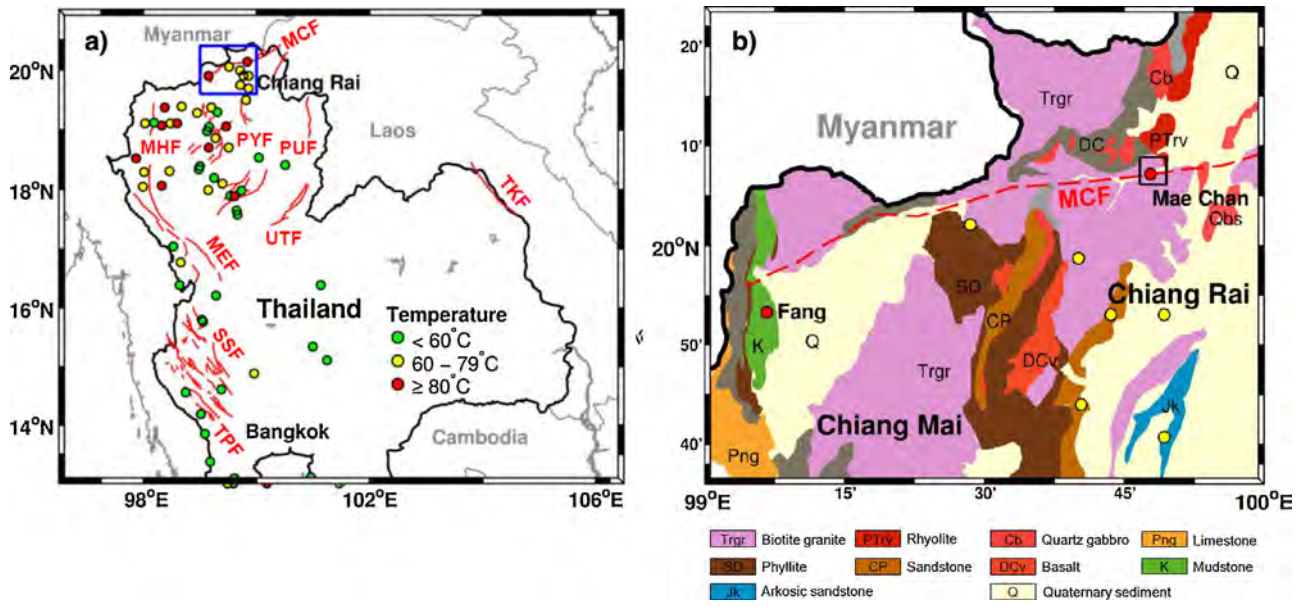
Fig. 1. (a) Locations of hot springs in northern Thailand in which red circles indicate the hot springs whose temperature exceeds 80 °C, yellow circles for temperature between 60 °C and 79 °C, and green for lower than 60 °C (Subtavewung et al., 2005). MCF, MHF, PYF, PUF, UTF, MEF, SSF, TPF, and TKF are for Mae Chan Fault, Mae Hong Son Fault, Pha Yoa Fault, Pua Fault, Uttaradit Fault, Moei Fault, Sri Sawat Fault, Three Pagoda Fault and Tha Khaek, respectively (after Kosuwan et al., 2006). (b) The detailed regional geological map of the blue rectangular block shown in (a). MCF is drawn according to Kosuwan and Lumjuan (1998). The "black" rectangular block indicates the area of the Mae Chan survey of this paper and is shown in detail in Fig. 2. (For interpretation of the references to colour in this figure legend, the reader is referred to the web version of this article.)

that the thermal water forms a shallow reservoir within the weathered, fractured granite and in the sedimentary basin and seeps to the surface through the Mae Chan Fault (Fig. 2). To further investigate the reservoir, vertical electrical sounding (VES) (DEDE, 2005; Thienprasert and Raksaskulwong, 1997; Thienprasert, 1980) and seismic refraction surveys (Thienprasert, 1980) including drilled holes (DEDE, 2005; Geotermica Italiana SRI, 1984; Owens, 2012; Thienprasert and Raksaskulwong, 1997) were conducted in the Mae Chan valley just near the hot springs (Y2 of Fig. 2). These studies indicated that the subsurface geology near Y2 consisted of a 10–20 m thick clay and sand layer above a 100 m thick weathered and fractured granite layer. At greater depths granite bedrock was encountered.

Even though spring temperatures can reach 99.5 °C (Singharajwarapan et al., 2012), the maximum temperature

Fig. 2. Locations of seven MT sites (crosses sign) covering an area of 3 km × 4 km in Mae Chan district, Chiang Rai province, Thailand. Geological rock units and topography are plotted as the background on this map. Y1 and Y4 are the hot spring locations found at the river bed. Y2 is the drilled hole (DEDE, 2005), and Y3a and Y3b are the hot springs found at the surface. Additional hot springs are also found around the north of MCH3 but are not shown.

reached at a depth of 100 m was 122 °C (Owens, 2012). In 2004, the area (Y2 of Fig. 2) was again drilled to a depth of 56 m to extract the hot fluid. Its temperature at that depth is around 94 °C (DEDE, 2005). The hot water is currently used for spas and drying agricultural products. In the initial assessments of the Mae Chan region, Owens (2012) concluded that the shallow fluids are not hot enough to generate electricity and drilling to depths of 1 km in the granite was not cost-effective. To assess the size of the reservoir without costly drilling, a magnetotelluric (MT) survey was conducted. The MT surveys are widely used in the past decades in geothermal exploration to reveal hydrothermal systems beneath the surface and to help define the drilling locations for the production wells (Heise et al., 2008; Newman et al., 2008). This is because of its major advantage as it is the only method that can directly sense a geothermal reservoir from its electrical resistivity from the surface down to depths of several kilometers (Árnason et al., 2010; Sinharay et al., 2010; Yu and Strack, 2010; Heise et al., 2008; Garg et al., 2007; Santos et al., 2007; Harinarayana et al., 2006; Uchida et al., 2005; Volpi et al., 2003; Lugão et al., 2002; Cumming et al., 2000; Bibby et al., 1995; Sandberg and Hohmann, 1982).

In this paper, we report on the analysis of a pilot MT survey in the Mae Chan area. The objectives of the experiment are to determine the source of the hot fluid and its location, and the size and depth of the reservoir. This information will be used to help determine the potential of the Mae Chan region for geothermal power production. We first describe the acquisition of the magnetotelluric data. Data processing, inversion and interpretation are then discussed.

2. Magnetotelluric survey: data acquisition, data processing and 3-D inversion

In July 2013, high frequency and broadband MT data were acquired at seven sites in a 3 km × 4 km area in the Mae Chan region which included many of the hot springs (Fig. 2). All sites used a KMS-820 data acquisition unit and coils and electrodes from KMS Technologies – KJT Enterprises Inc., Houston, TX, USA. Only the
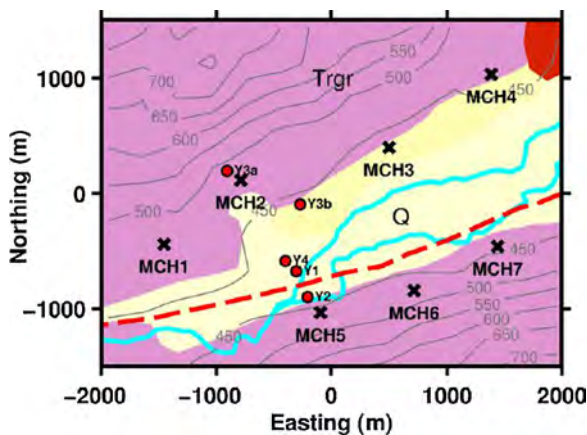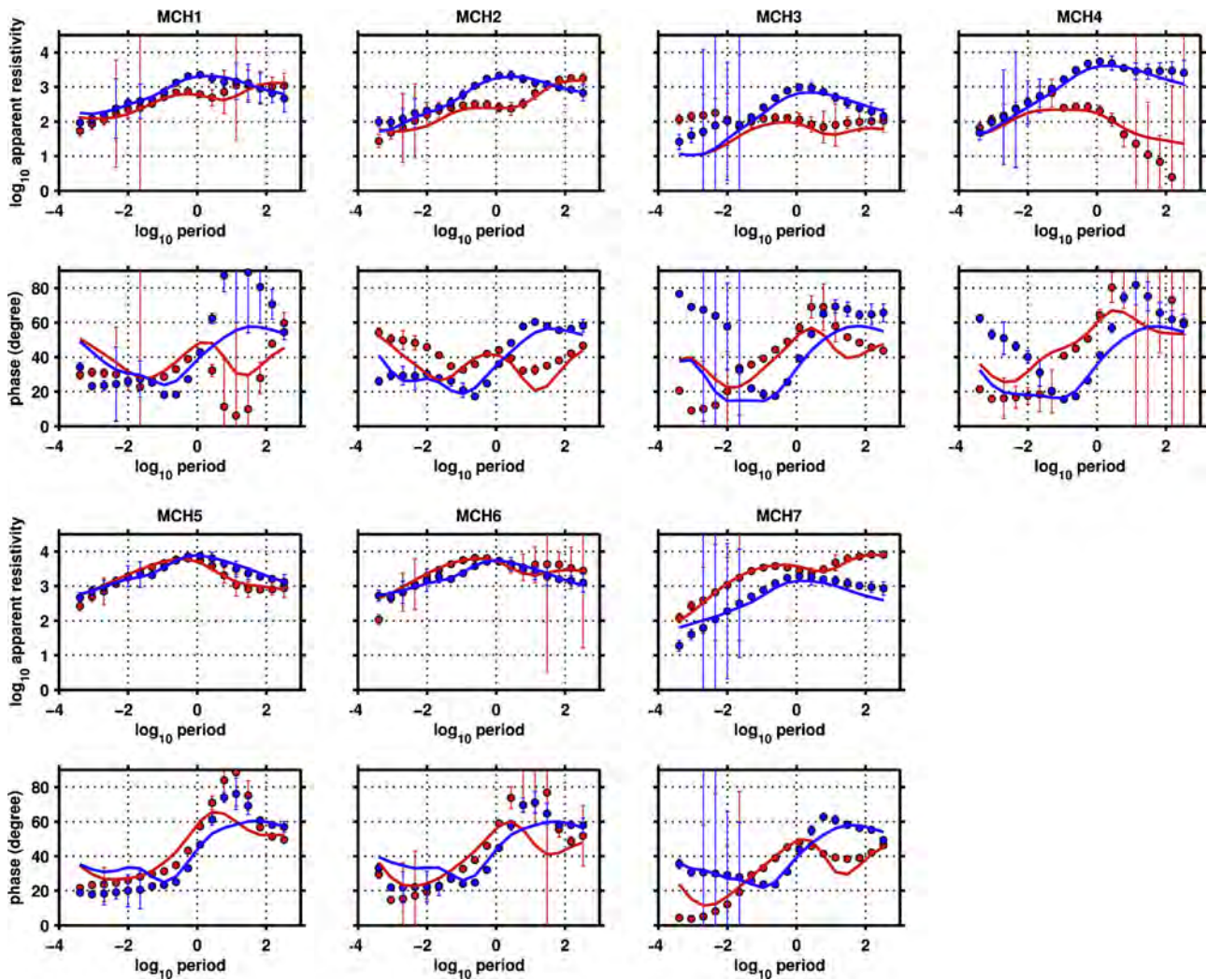
Fig. 3. The apparent resistivities (ohm m) and phases (degree) as a function of $\log_{10}$ periods (second) computed from the off-diagonal impedance tensor at seven locations acquired in the locations shown in Fig. 2. Red is xy and blue is yx mode. The circles and error bars are from field measurement, and the solid lines are the calculated responses generated from the inverted model shown in Figs. 5–7. (For interpretation of the references to colour in this figure legend, the reader is referred to the web version of this article.)

horizontal electric and magnetic fields (E_x, E_y, H_x and H_y) were measured, where x is oriented north and y is oriented east. The electrodes (LEMI-701), broadband magnetic coils (LEMI-120) and the acquisition unit were left overnight to acquire the data for a total of about 20 h at each station (2 h of 1000 Hz sampling rate and 18 h of 250 Hz sampling rate). For the high frequency magnetic fields, the broadband coils LEMI-120 were replaced with the high frequency coils (LEMI-118) and data was acquired 30 min before or after the 20-h measurement using a sampling rate of 10,000 Hz. Both broadband and high frequency data were processed and combined to produce data ranging from 5000 Hz to around 1000 s.

Most of the sites are less than 10 km from the main district of Mae Chan where its population is less than 20,000. Cultural noise from electric cables and telephone poles in villages and resorts can dominate the data in some period ranges. In order to improve the quality of the data, a remote reference site (Gamble et al., 1979) was installed in the Fang district, Chiang Mai province, about 70 km southwest of the survey area. Similar sets of sampling rates were used at the reference site to acquire the broadband data simultaneously with the local sites. Due to the lack of another pair of LEMI-118 high frequency magnetic coils, we could not acquire the high frequency data at the remote reference site. The broadband data from 500 Hz and lower (or longer periods) was

therefore processed with remote reference techniques using KMS processing software based on robust multiple-station processing (Egbert, 1997), while the high frequency data from 5000 Hz to 500 Hz was only locally processed without remote reference data.

Because the high frequency data were not remotely processed and the data quality was poor, the data above 3000 Hz were omitted. Similarly, the data above 300 s are generally contaminated and were also omitted from the inversion process as they also correspond to structures that are deeper than the region of interest. As in other areas around the world, the data in the dead band (periods of 1–100 s) is relatively poor due to low signal. For the inversion, the combined and processed impedance tensor Z from periods ranging from 3000 Hz to 300 s was selected linearly on a $\log_{10}$ scale to give a total of 18 periods per site. The conversion of the impedance tensor to the apparent resistivity and phase of the xy- and yx- polarizations along with the error bars for each station are shown in Fig. 3.

The parallel version of WSINV3DMT (Siripunvaraporn and Egbert, 2009; Siripunvaraporn et al., 2005) was used to invert the selected impedance tensor Z. The code has been widely used in many geothermal explorations (Árnason et al., 2010; Bertrand et al., 2013; Ghaedrahmati et al., 2013; Heise et al., 2008; Patro and Egbert, 2011; Tuncer et al., 2006). One major advantage of directly performing the 3-D inversion is that there is no requirement to
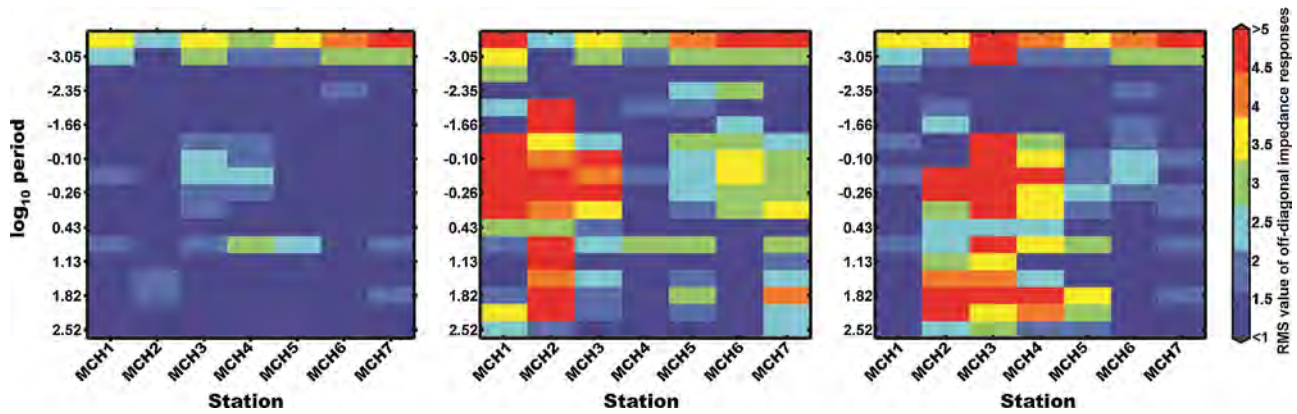
Fig. 4. RMS misfit maps show the misfit between the observed data and the calculated data of each site as a function of period. The calculated data are obtained (a) from the inverted model shown in Fig. 5; (b) by replacing the C1 conductor of Fig. 5 with a 300 Ω m zone; and (c) by replacing the C2 conductor of Fig. 5 with a 300 Ω m zone.

conduct the dimensionality analysis (Siripunvaraporn, 2012). Since Z_{xx} and Z_{yy} are more severely distorted, only the off-diagonal data, Z_{xy} and Z_{yx}, were used for the 3-D inversion to reduce the risk of producing artifacts in the inverted model. The minimum error floor was set at 5% of the $|Z_{xy}Z_{yx}|^{1/2}$. For the outliers, the error bars were increased to be large enough relative to the neighboring data. The area with topography was discretized into a $49 \times 52 \times 67$ grid in north-south, east-west and depth, respectively. For the vertical mesh, the first layer is discretized at 30 m to provide high accuracy responses for all data. The thickness of the subsequent layers increases by 1.5–1.8 times of the previous layers. The horizontal grid sizes in the survey region are 200 m on both directions. The model mesh outside of the investigation area was extended using a logarithmic scale to avoid boundary effects.

The inversion was run multiple times with different starting parameters. The preferred inversion result was obtained by using a 300 Ω m half-space as the initial model to produce the normalized RMS misfit of about 4.6. After 4 iterations, the misfit level decreased to about 1.6 RMS. This step was run with a larger length-scale parameter in the WSINV3DMT code (Siripunvaraporn et al., 2005; Siripunvaraporn and Egbert, 2009) to model the large scale structures that are required by the observed data. To further decrease the RMS level, a smaller length-scale was therefore used to allow the smaller features required by the data to be added in the inverted model, as with the techniques used in Boonchaisuk et al. (2013). The reduced length-scale inversion step also helps to fit the data that are affected by static distortion (Siripunvaraporn, 2012). After 2 more iterations of the inversion, this time starting from the previous model but with smaller length scale, the misfit level was stabilized at 1.5 RMS. At that point, we terminated the inversion. The observed data and the calculated responses from all 7 stations are shown in Fig. 3. The RMS misfits for each site and each period for this run are shown in Fig. 4a. The final inversion model is plotted in a plan view in Fig. 5 and in cross-sections in Figs. 6 and 7.

Three main features are shown in Figs. 5–7: the conductive zones C1 and C2 and the resistive structure labeled as R. All of these features also appear in other models with different inversion parameters inferring that they are required by the data. The conductor C1 is surrounded with MCH1, MCH2, MCH3, MCH5 and MCH6 sites, while conductor C2 is only enclosed by MCH2, MCH3 and MCH4 sites on just its southern side. The size and thickness of C2 might therefore be less constrained than those of C1. More stations located on the northern side may be necessary in order to further constrain C2. The conductive zones C1 and C2 are of particular interest because they can be linked to the geothermal reservoir discussed in the following section. We therefore do the feasibility tests in order to validate that C1 and C2 are required by the observed data.

To verify the existence of C1, the conductive volume C1 of the inverted model in Figs. 5–7 was replaced by a background resistivity of 300 Ω m and ran the forward modeling to fit the observed data. We found that the overall RMS dramatically increased to 3.4 indicating a poorer fit to the observed data. A similar experiment was conducted with the C2 zone. After the forward modeling run of the model without the C2 conductive zone, the overall RMS misfit increased to 3.1. Both of these experiments indicate us that both conductive C1 and C2 zones are required by the observed data. For a detailed investigation, Fig. 4b and c shows the RMS misfit of each site and each period after replacing C1 and C2, respectively, with a background resistivity of 300 Ω m. Fig. 4b shows that C1 is required by most sites, particularly MCH1, MCH2 and MCH3 as removing it results in a higher RMS misfit. The period range that senses conductor C1 is around 0.03–10 s. Fig. 4c shows that conductor C2 is required by MCH2, MCH3 and MCH4. The period range affecting C2 is slightly larger (around 0.03–100 s), which might be why C2 is interpreted to be thicker and deeper than C1.

3. Interpretation and discussion

The previous section shows that the final inverted model (Figs. 5–7) contains three prominent features: the shallow conductive zones, C1 and C2, the resistive structure, R, and the resistivity contrast between the conductive zones and the resistive block matches the Mae Chan Fault well (drawn as the dashed line in Fig. 5). In this section, we link these prominent features with the geology of the area.

The two conductive zones C1 and C2 form a thin conductive layer near the surface covering the Mae Chan valley (Fig. 5a) but separate into two zones below 50 m depth (e.g., Figs. 5b and 6a). C1 conductor dissipates at around 250 m while C2 continues to a depth of 500 m (Fig. 6a). C2 covers a larger area (around 1 km²). C1 and C2 are located within the Quaternary alluvium. The center of C1 is close to where the hot springs seep into the Mae Chan creek (indicated by Y1 and Y4 in Fig. 5) and also the drilled hole (indicated by Y2), while the center of C2 is associated with hot fluid emerging at the surface. Two hot springs (Y3a and Y3b) are also found between C1 and C2. Since there is a correlation between the hot springs and the conductors beneath, we can therefore suggest that C1 and C2 are reservoirs for the hot fluid. The reservoirs are connected in the top sedimentary deposits in the north of MCF (Figs. 5a, 6 and 7). They become separated on entering the weathered and fractured granite below (Figs. 6 and 7).

The resistor R appears in the southern region near stations MCH5, MCH6 and MCH7 (Fig. 5). It extends from surface to cover the entire survey area at a greater depth as clearly displayed in
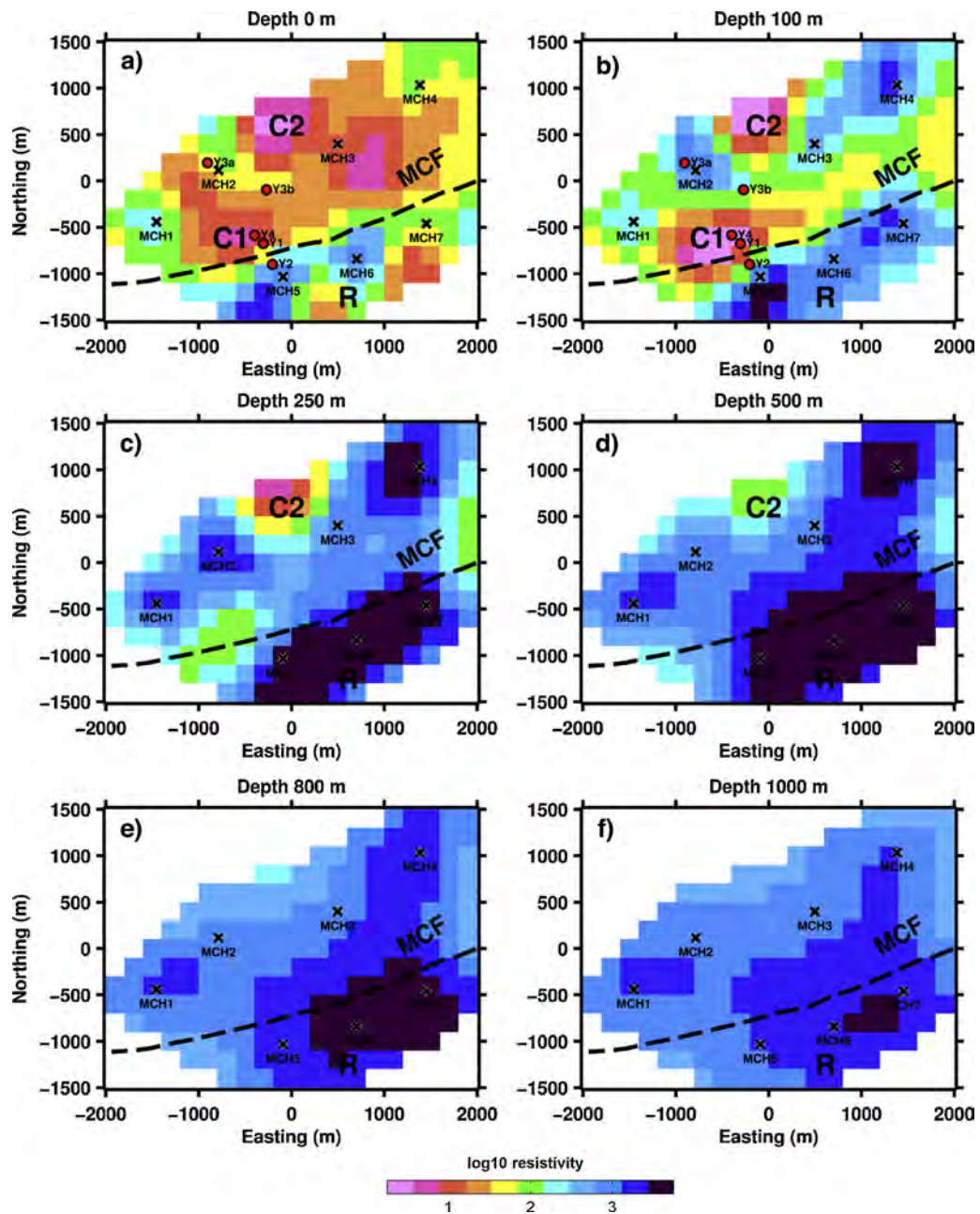
Fig. 5. The plane-view of the final inverted model at (a) surface, (b) 100 m, (c) 250 m, (d) 500 m, (e) 800 m and (f) 1000 m depths. MT locations and their name are marked as crosses. Mae Chan Fault (MCF) is drawn as a dashed line. C1 and C2 are the two conductive zones while R is the resistivity zone. They are only marked where they appear in the model.

Figs. 6 and 7. According to prior geological information (Kosuwan and Lumjuan, 1998) and the surface geology map (Fig. 1b), the resistive body R corresponds to the batholith Triassic granite. As its value is moderately high, 1000–3000 Ω m, it is interpreted as being unweathered granite. In the north, part of the weathered and fractured granite along with the sedimentary layer is interpreted to be filled with the hot fluid, which produces the low resistivity zones C1 and C2 (Fig. 5). As with other non-volcanic geothermal systems in granitic rocks (Gianelli et al., 1997; Harinarayana et al., 2006; Newman et al., 2008; Santos, 1997; Uchida et al., 2005), the heat source for the hot fluid in the Mae Chan region should come from the batholith granite R at great depth. When the rain water infiltrates into the ground, the ground water is heated by the hotter batholith resulting from the decay of radioactive elements of

the minerals in the granite. The hot water then rises to the surface along faults and fractures.

Using the resistivity curve versus temperature developed for two granite bodies in Japan (Llera et al., 1990), we can roughly estimate the temperature of the granite in our area where its mean resistivity is 1000 Ω m in the upper 5 km depth to be around 130 °C. Although the granite in our area is different in composition than the granite described by Llera et al. (1990), the estimated temperature value of 130 °C agrees well with temperatures of 122 °C and 127 °C calculated using the chalcedony and K-Mg geothermometers (Singharajwarapan et al., 2012). In addition, the resistivity of the hot granite tends to decrease at depth of more than 5 km. A decrease in resistivity may correspond to an increase in temperature as reported in many publications (Akpan et al., 2013; Árnason
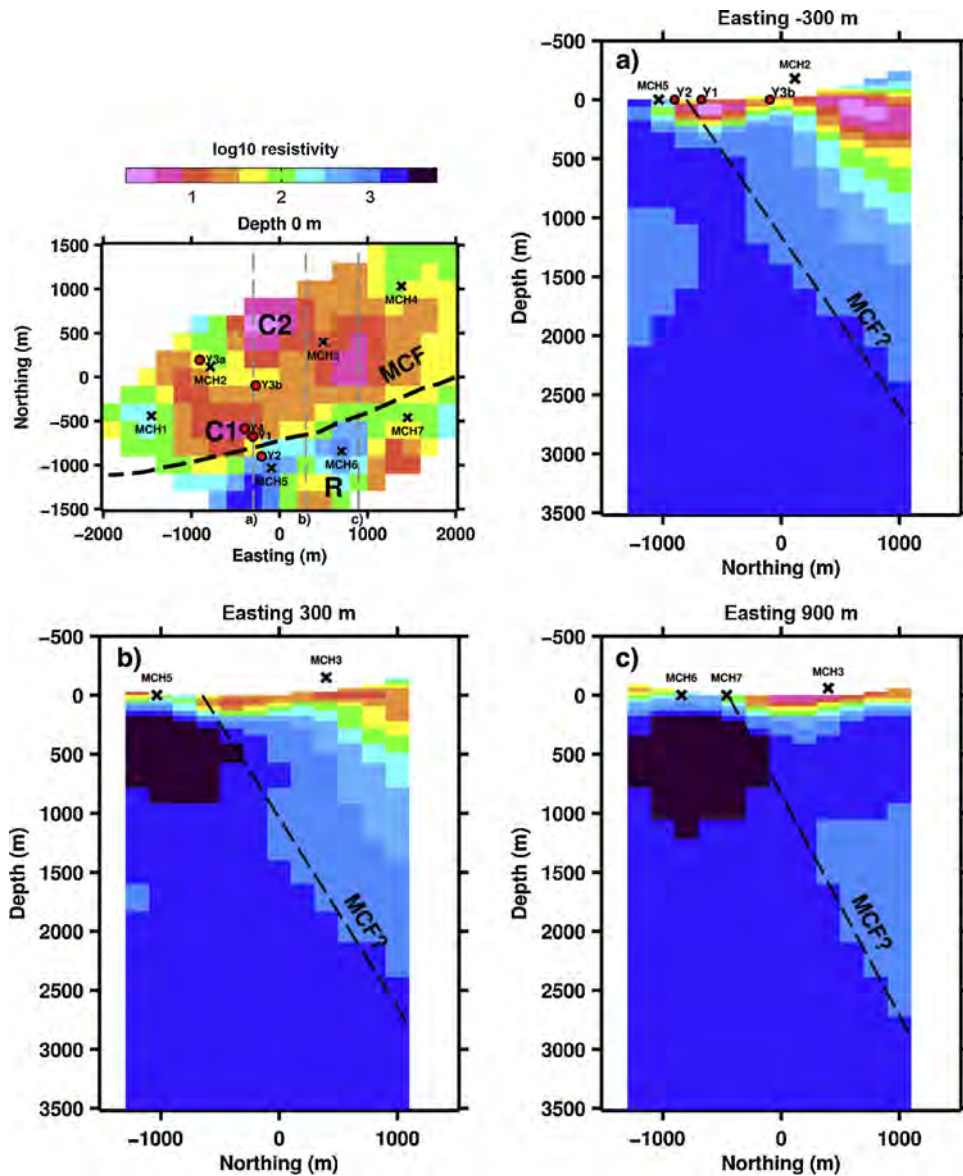
Fig. 6. North-south cross-section of the final inverted model (Fig. 5a) at east-west distances of (a) −300 m, (b) 300 m and (c) 900 m. The dashed line is the estimated orientation of the Mae Chan Fault (MCF). Locations of the MT stations are also mapped and shown at the surface along with the hot spring locations.

et al., 2010; Harinarayana et al., 2006; Nover, 2005; Llera et al., 1990; Olhoeft, 1981; Shankland and Ander, 1983).

Another feature that can be observed in our inverted model is the resistivity contrast between the conductive features C1 and C2 in the north and the resistive zone R in the south which is oriented in the northwest-southeast direction. The location of the abrupt change of the resistivity occurs at the Mae Chan Fault mapped by Kosuwan and Lumjuan (1998). The contrast is therefore interpreted as the fault line cutting through the granite in the middle of the survey area. The contrast vanishes at depth as shown in the cross-sections of Fig. 6a–c. By following the resistivity contrast from the fault trace at the surface (Fig. 2) to greater depths (Fig. 6a–c), we can infer that the Mae Chan Fault dips at 40–60° which is not as steep as expected (Fenton et al., 2003; Kosuwan and Lumjuan, 1998). Its hanging wall is in the north and consists of a sedimentary deposit and weathered and fractured granite on top of the unweathered granite. The foot wall is in the south and consists of mostly batholith granite. Below 2 km, both sides of the fault have the same resistivity suggesting granite forms both sides of the fault. Further detailed surveys with MT stations closer than the current

spacing of 1 km are needed to better define the fault location at depth.

This study helps confirm the study of Owens (2012) that the heat source for the Mae Chan hot springs is the hot granite. The reservoir is located within the first few hundred meters from the surface in the sedimentary deposits and weathered and fractured granite. Based on our study, the hot fluid in the C1 conductor can be considered as a potential area to develop a small-scale binary geothermal power plant similar to the 300 kW plant in the Fang district or a novel low enthalpy binary geothermal power plant (Gabbrielli, 2012). However, the reservoir appears relatively small. A lack of balance between usage and re-injection could distort the shallow hydrology of the area (Heise et al., 2008). The C2 conductor should be drilled to determine if the temperature of the hot fluid is high enough for development.

A larger scale geothermal power plant using the hot granite at a great depth is also possible. However, little is known about the granite at depth. This would require further measurements as our first phase of the MT survey covered only 10 km² which is a small part of the whole batholith exposed at the surface. Expanding the
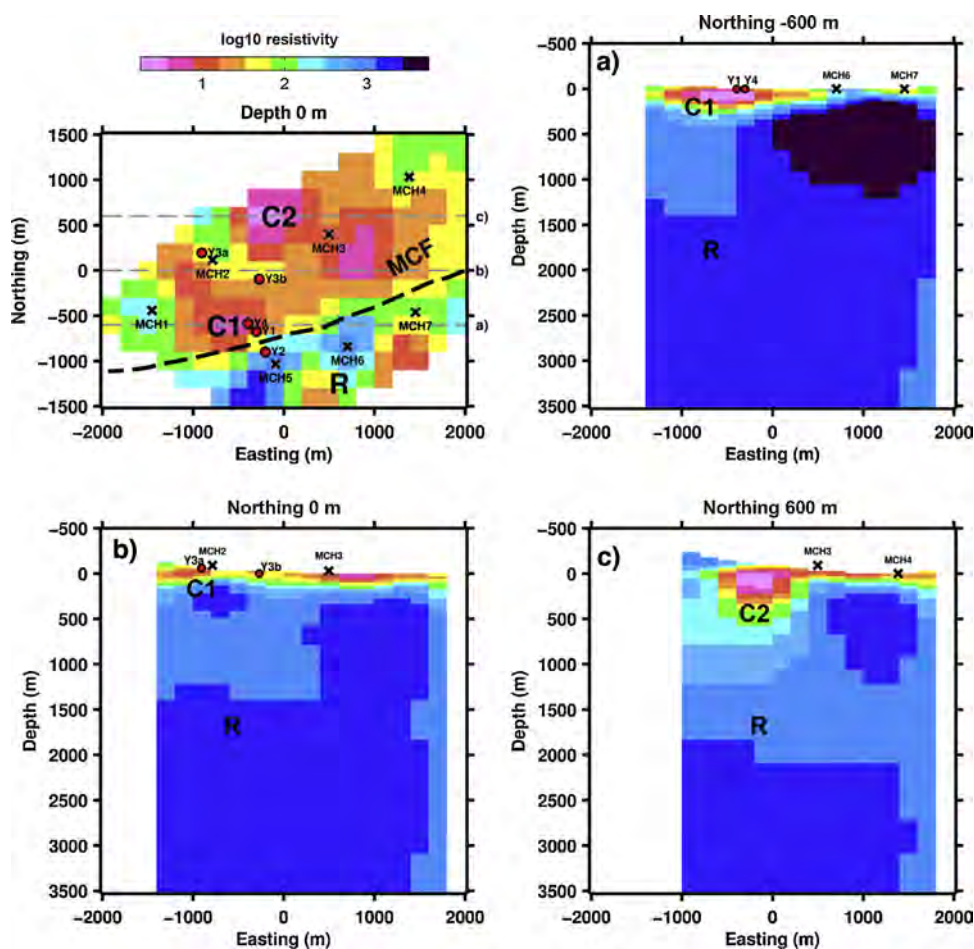
Fig. 7. East-west cross-section of the final inverted model (Fig. 5a) at north-south distances of (a) −600 m, (b) 0 m and (c) 600 m. Locations of the MT stations are also mapped and shown at the surface along with the hot spring locations.

MT site coverage to a larger scale may show the existence of permeable fractured granite at great depth which could be used for geothermal power. A combination with thermal gradient drilling would require assessing the granite potential.

4. Conclusion

A 3-D resistivity structure determined from a small number of MT stations sparsely distributed around the Mae Chan geothermal area provides very useful information to assess the potential for a geothermal power plant. In the Mae Chan hydrothermal system, hot fluid heated from the deeper granitic batholith, identified as high resistivity feature R, is stored in the fractured and weathered granite and the sedimentary rock indicated by two conductive zones C1 and C2. A fracture in the damaged zone of the fault (shown as a resistivity contrast) allows the pressurized hot fluid to reach the surface. Since the temperature of the Mae Chan hydrothermal system does not seem to be high, we propose the development of small-scale geothermal power plants over the two zones C1 and C2. Further detailed investigation with more MT coverage along with deep well drilling may be necessary in order to assess the potential to build a larger scale geothermal power plant in the area.

References

Akpan, A.E., Narayanan, M., Harinarayana, T., 2013. Estimation of subsurface temperatures in the Tattapani geothermal field, central India from limited volume of magnetotelluric data and borehole thermograms using a constructive back-propagation neural network. Earth Interact., http://dx.doi.org/10.1175/2013EI000539.1 (in press).

Árnason, K., Eysteinsson, H., Hersir, G.P., 2010. Joint 1D inversion of TEM and MT data and 3D inversion of MT data in the Hengill area, SW Iceland. Geothermics 39, 13–34, http://dx.doi.org/10.1016/j.geothermics.2010.01.002.

Barr, S.M., Ratanasathien, B., Breen, D., Ramingwong, T., Sertsrivanit, S., 1979. Hot springs and geothermal gradients in northern Thailand. Geothermics 8, 85–95, http://dx.doi.org/10.1016/0375-6505(79)90002-6.

Bertrand, E., Caldwell, T.G., Hill, G.J., Bennie, S.L., 2013. 3-D inversion of a 200+ site magnetotelluric array for deep geothermal exploration. In: 5th International Symposium on Three-Dimensional Electromagnetics, Sapporo, Japan, May 7–9, 2013, p. 3.

Bibby, H.M., Caldwell, T.G., Davey, F.J., Webb, T.H., 1995. Geophysical evidence on the structure of the Taupo volcanic zone and its hydrothermal circulation. J. Volcanol. Geotherm. Res. 68, 29–58, http://dx.doi.org/10.1016/0377-0273(95)00007-H.

Boonchaisuk, S., Siripunvaraporn, W., Ogawa, Y., 2013. Evidence for middle Triassic to Miocene dual subduction zones beneath the Shan-Thai terrane, western Thailand from magnetotelluric data. Gondwana Res. 23, 1607–1616.

Cumming, W., Nordquist, G., Astra, D., 2000. Geophysical exploration for geothermal resources: an application for combined MT-TDEM. In: Society of Exploration Geophysicists Annual Meeting Technical Program Expanded Abstracts, 6–11 August, Calgary, Canada, pp. 1071–1074.

Chuaviroj, S., 1988. Geothermal development in Thailand. Geothermics 17, 421–428, http://dx.doi.org/10.1016/0375-6505(88)90071-5.

DEDE (Thailand Department of Alternative Energy Development and Efficiency), 2005. Hot Spring Development Project at Mae Chan – ChiangRai. DEDE, pp. 177, Available at: http://www3.dede.go.th/dede/fileadmin/upload/pic-tures_eng/Webpage_MaeChan_HotSpring.pdf

Egbert, G.D., 1997. Robust multiple-station magnetotelluric data processing. Geophys. J. Int. 130, 475–496, http://dx.doi.org/10.1111/j.1365-246X.1997.tb05663.x.

Fenton, C., Charusiri, P., Wood, S., Boise, I., 2003. Recent paleoseismic investigations in Northern and Western Thailand. Ann. Geophys. 46, 957–981, http://dx.doi.org/10.4401/ag-3464.

Gabbrielli, R., 2012. A novel design approach for small scale low enthalpy binary geothermal power plants. Energy Convers. Manag. 64, 263–272, http://dx.doi.org/10.1016/j.enconman.2012.04.017.

Gamble, T.D., Goubau, W.M., Clarke, J., 1979. Magnetotellurics with a remote magnetic reference. Geophysics 44, 53–68, http://dx.doi.org/10.1190/1.1440923.

Garg, S.K., Pritchett, J.W., Wannamaker, P.E., Combs, J., 2007. Characterization of geothermal reservoirs with electrical surveys: beowawe geothermal field. Geothermics 36, 487–517, http://dx.doi.org/10.1016/j.geothermics.2007.07.005.

Geotermica Italiana SRI, 1984. Geothermal Reconnaissance Survey of Northern Thailand-Final Report, Geology, Pisa, Italy., pp. 86 (unpublished report).

Ghaedrahmati, R., Moradzadeh, A., Fathianpour, N., Lee, S.K., Porkhial, S., 2013. 3-D inversion of MT data from the Sabalan geothermal field, Ardabil, Iran. J. Appl. Geophys. 93, 12–24, http://dx.doi.org/10.1016/j.jappgeo.2013.03.006.

Gianelli, G., Manzella, A., Puxeddu, M., 1997. Crustal models of the geothermal areas of southern Tuscany (Italy). Tectonophysics 281, 221–239, http://dx.doi.org/10.1016/S0040-1951(97)00101-7.

Harinarayana, T., Abdul Azeez, K.K.K., Murthy, D.N.N., Veeraswamy, K., Eknath Rao, S.P.P., Manoj, C., Naganjaneyulu, K., 2006. Exploration of geothermal structure in Puga geothermal field, Ladakh Himalayas, India by magnetotelluric studies. J. Appl. Gerontol. 58, 280–295, http://dx.doi.org/10.1016/j.jappgeo.2005.05.005.

Heise, W., Caldwell, T.G., Bibby, H.M., Bannister, S.C., 2008. Three-dimensional modelling of magnetotelluric data from the Rotokawa geothermal field, Taupo Volcanic Zone. N. Z. Geophys. J. Int. 173, 740–750, http://dx.doi.org/10.1111/j.1365-246X.2008.03737.x.

Kosuwan, S., Lumjuan, A., 1998. Neotectonics of Mae Chan Fault in Mae Chan district, Chiang Rai Province. Department of Mineral Resources, pp. 56.

Kosuwan, S., Takashima, I., Charusiri, P., 2006. Active Fault Zones in Thailand [WWW Document]. Department of Mineral Resources, http://www.dmr.go.th/main.php?filename=fault_En

Llera, F., Sato, M., Nakatsuka, K., Yokoyama, H., 1990. Temperature dependence of the electrical resistivity of water-saturated rocks. Geophysics 55, 576–585.

Lugão, P.P., LaTerra, E.F., Kriegshäuser, B., Fontes, S.L., 2002. Magnetotelluric studies of the Caldas Novas geothermal reservoir. Braz. J. Appl. Geophys. 49, 33–46, http://dx.doi.org/10.1190/1.1442869.

Newman, G.A., Gasperikova, E., Hoversten, G.M., Wannamaker, P.E., 2008. Three-dimensional magnetotelluric characterization of the Coso geothermal field. Geothermics 37, 369–399, http://dx.doi.org/10.1016/j.geothermics.2008.02.006.

Nover, G., 2005. Electrical properties of crustal and mantle rocks – a review of laboratory measurements and their explanation. Surv. Geophys. 26, 593–651, http://dx.doi.org/10.1007/s10712-005-1759-6.

Olhoeft, G., 1981. Electrical properties of granite with implications for the lower crust. J. Geophys. Res. 86, 931–936, http://dx.doi.org/10.1029/JB086iB02p00931.

Owens, L., 2012. Initial Assesments of High Potential Geothermal Sites in Northern Thailand. Ormat Technologies, Inc., NV, USA, pp. 8 (unpublished report).

Patro, P.K., Egbert, G.D., 2011. Application of 3D inversion to magnetotelluric profile data from the Deccan Volcanic Province of Western India. Phys. Earth Planet. Inter. 187, 33–46, http://dx.doi.org/10.1016/j.pepi.2011.04.005.

Raksaskulwong, M., 2008. Thailand geothermal energy: development history and current status. In: Proceedings of the 8th Asian Geothermal Symposium, pp. 39–46.

Ramingwong, T., Lertsrimongkol, S., Asnachinda, P., Praserdvigai, S., 2000. Update on Thailand geothermal energy research and development. In: World Geothermal Congress, pp. 377–386.

Sandberg, S., Hohmann, G., 1982. Controlled-source audiomagnetotellurics in geothermal exploration. Geophysics 47, 100–116, http://dx.doi.org/10.2172/6749290.

Santos, F.M., Afonso, A.R.A., Dupis, A., 2007. 2D joint inversion of dc and scalar audio-magnetotelluric data in the evaluation of low enthalpy geothermal fields. J. Geophys. Eng. 4, 53–62, http://dx.doi.org/10.1088/1742-2132/4/1/007.

Santos, F.M., 1997. Study of the Chaves geothermal field using 3D resistivity modeling. J. Appl. Gerontol. 37, 85–102, http://dx.doi.org/10.1016/S0926-9851(97)00010-4.

Shankland, T.J., Ander, M.E., 1983. Electrical conductivity, temperatures, and fluids in the lower crust. J. Geophys. Res. 88, 9475, http://dx.doi.org/10.1029/JB088iB11p09475.

Singharajwarapan, F.S., Wood, S.H., Prommakorn, N., Owens, L., 2012. Northern Thailand geothermal resources and development: a review and 2012 update. GRC Trans. 36, 787–791.

Sinharay, R.K.R., Srivastava, S., Bhattacharya, B.B.B., 2010. Audiomagnetotelluric studies to trace the hydrological system of thermal fluid flow of Bakreswar Hot Spring, Eastern India: a case history. Geophysics 75, B187–B195, http://dx.doi.org/10.1190/1.3431532.

Siripunvaraporn, W., 2012. Three-dimensional magnetotelluric inversion: an introductory guide for developers and users. Surv. Geophys. 33, 5–27, http://dx.doi.org/10.1007/s10712-011-9122-6.

Siripunvaraporn, W., Egbert, G., 2009. WSINV3DMT: vertical magnetic field transfer function inversion and parallel implementation. Phys. Earth Planet. Inter. 173, 317–329, http://dx.doi.org/10.1016/j.pepi.2009.01.013.

Siripunvaraporn, W., Egbert, G., Lenbury, Y., Uyeshima, M., 2005. Three-dimensional magnetotelluric inversion: data-space method. Phys. Earth Planet. Inter. 150, 3–14, http://dx.doi.org/10.1016/j.pepi.2004.08.023.

Subtavewung, P., Raksaskulwong, M., Tulyatid, J., 2005. The characteristic and classification of hot springs in Thailand. In: Proceedings World Geothermal Congress, p. 7.

Thienprasert, A., 1980. Mae Chan Geothermal Energy Resource, Gephysical Investigations Resistivity Method. Seismic Refraction Method and One meter Depth Temperature Reading Method. Department of Mineral Resources, pp. 68.

Thienprasert, A., Raksaskulwong, M., 1997. Resistivity and Heat Flow Studies at Mae Chan Geothermal Area, Chiangrai Province. Department of Mineral Resources, pp. 12 (online) library.dmr.go.th.

Tuncer, V., Unsworth, M., Siripunvaraporn, W., Craven, J., 2006. Exploration for unconformity-type uranium deposits with audiomagnetotelluric data: a case study from the McArthur River mine, Saskatchewan, Canada. Geophysics 71, B201–B209, http://dx.doi.org/10.1190/1.2348780.

Uchida, T., Song, Y., Lee, T., 2005. Magnetotelluric survey in an extremely noisy environment at the Pohang low-enthalpy geothermal area, Korea. In: Proceedings World Geothermal Congress, pp. 24–29.

Volpi, G., Manzella, A., Fiordelisi, A., 2003. Investigation of geothermal structures by magnetotellurics (MT): an example from the Mt. Amiata area, Italy. Geothermics 32, 131–145.

Yu, G., Strack, K., 2010. Integrated MT/Gravity geothermal exploration in Hungary: a success story. In: 21st ASEG Conference and Exhibition, Sydney, Australia, p. 3.